ELSEVIER

Nanomedicine: Nanotechnology, Biology, and Medicine
xx (2017) xxx–xxx

nanomedicine
Nanotechnology, Biology, and Medicine

nanomedjournal.com

Nanoparticle-mediated radiopharmaceutical-excited fluorescence molecular imaging allows precise image-guided tumor-removal surgery

Zhenhua Hu[a,b,*], Chongwei Chi[a], Muhan Liu[a], Hongbo Guo[a], Zeyu Zhang[a], Chaoting Zeng[a], Jinzuo Ye[a], Jing Wang[c], Jie Tian[a,b,*], Weidong Yang[c,**], Wanhai Xu[d,***]

[a]*Key Laboratory of Molecular Imaging of Chinese Academy of Sciences, Institute of Automation, Chinese Academy of Sciences, Beijing, China*
[b]*The State Key Laboratory of Management and Control for Complex Systems, Institute of Automation, Chinese Academy of Sciences, Beijing, China*
[c]*Department of Nuclear Medicine, Xijing Hospital, Fourth Military Medical University, Xi'an, China*
[d]*Department of Urinary Surgery, the Fourth Affiliated Hospital of Harbin Medical University, Harbin, China*

Received 7 December 2016; accepted 2 January 2017

Abstract

Fluorescent molecular imaging technique has been actively explored for optical image-guided cancer surgery in pre-clinical and clinical research and has attracted many attentions. However, the efficacy of the fluorescent image-guided cancer surgery can be compromised by the low signal-to-noise ratio caused by the external light excitation. This study presents a novel nanoparticle-mediated radiopharmaceutical-excited fluorescent (REF) image-guided cancer surgery strategy, which employs the internal dual-excitation of europium oxide nanoparticles through both gamma rays and Cerenkov luminescence emitted from radiopharmaceuticals. The performance of the novel image-guided surgery technique was systematically evaluated using subcutaneous breast cancer 4 T1 tumor models, orthotropic and orthotropic-ectopic hepatocellular carcinoma tumor-bearing mice. The results reveal that the novel REF image-guided cancer surgery technique exhibits high performance of detecting invisible ultra-small size tumor (even less than 1 mm) and residual tumor tissue. Our study demonstrates the high potential of the novel image-guided cancer surgery for precise tumor resection.

Key words: Radiopharmaceutical-excited fluorescence imaging (REFI); Cerenkov luminescence imaging (CLI); Radionuclides; Hepatocellular carcinoma (HCC); Positron emitting tomography (PET)

Radical resection of cancer is the most effective method to improve the survival rate of cancer patients.[1] Precise removal of cancerous tissue avoids adverse events and systemic toxicity, prevents damage of healthy tissues, and decreases the risk of postoperative complications.[2] Presently, optical image-guided cancer surgery, especially fluorescence molecular imaging (FMI) guided surgery, has attracted intensive attentions and has been actively explored in pre-clinical[3–5] and clinical research.[6–10] FMI has many advantages, such as no radiation, high sensitivity, high resolution, high specificity and real-time monitoring capability.[11] Numerous researches have shown that FMI can help resolve mouse lymphatic vasculature and sentinel lymph nodes near tumors,[3] delineate tumor margins,[4] improve intra-operative staging,[5] enable more radical cytoreduction,[6,7] detect ignored tumor lesions in some special organs,[8] map lymph node metastases better,[9,10] and so on. However, FMI could suffer from high background and thus low signal noise ratio (SNR) because of the use of external laser excitation.[12,13]

Funding: This study was funded by the National Natural Science Foundation of China Grant No. 81227901, the National Key Research and Development Program of China Grant No. 2016YFC0102600, the National Natural Science Foundation of China Grant No. 61622117, 81671759, 81371594, 61302024.

Conflict of Interest: The author declares that he/she has no conflict of interest.

Ethical approval: All applicable international, national, and/or institutional guidelines for the care and use of animals were followed.

*Correspondence to: Z. Hu and J. Tian, Key Laboratory of Molecular Imaging of Chinese Academy of Sciences, Institute of Automation, Chinese Academy of Sciences, Beijing, 100190, China.

**Correspondence to: W. Yang, Department of Nuclear Medicine, Xijing Hospital, Fourth Military Medical University, Xi'an, 710032, China.

***Correspondence to: W. Xu, Department of Urinary Surgery, the Fourth Affiliated Hospital of Harbin Medical University, Harbin, 150001, China.

E-mail addresses: zhenhua.hu@ia.ac.cn (Z. Hu), tian@ieee.org (J. Tian), yangwd1971@163.com (W. Yang), xuwanhai@163.com (W. Xu).

http://dx.doi.org/10.1016/j.nano.2017.01.005
1549-9634/

Moreover, very few fluorescent probes have been approved by the Food and Drug Administration (FDA) for clinical use.[11,14] All these problems could limit its wide clinical applications.

In recent years, Cerenkov luminescence imaging (CLI), which employs the Cerenkov radiation emitted from radiopharmaceuticals for optical imaging, arose as a new imaging modality and has found broad applications.[15–17] It can be used in development and evaluation of radiopharmaceuticals,[15–20] monitoring cancer drug therapy,[21,22] detecting the expression of tumor markers,[23–25] and so on. A wide variety of radionuclides and radiopharmaceuticals could serve as probes for CLI, besides using for positron emission tomography (PET) and single photon emission computed tomography (SPECT).[15,17] Importantly, CLI has been evaluated in clinical studies, including the imaging of human thyroid gland using ^{131}I[26] and the patients' lymph nodes in the axillary region by injection of ^{18}F–fluorodeoxyglucose (^{18}F–FDG).[27] Compared to FMI, CLI does not require the external light illumination, has lower auto-fluorescence and can take advantages of numerous FDA approved radiopharmaceuticals for clinical imaging. CLI has also been applied for the optical image-guided cancer surgery.[28–31] Liu *et al* have developed a Cerenkov luminescence endoscopy system and the *in vivo* tumor imaging study demonstrated the ability of CLI to guide the resection of tumor tissues. However, on the other hand, because the Cerenkov luminescence signal is very weak, it usually takes long time for optical imaging system to acquire the weak Cerenkov luminescence. Therefore it is hard to obtain good imaging contrast in living subjects and achieve real time image-guided surgery capability using CLI. 之前的研究成果

In this study, a novel radiopharmaceutical-excited fluorescence (REF) image-guided surgery strategy has been explored based on our previous work on the novel radiopharmaceuticals excited fluorescence imaging (REFI) technique. REFI involves the use of nanoparticles such as europium oxide (EO) nanoparticles that can be excited by photons and radiopharmaceuticals such as ^{18}F–FDG to generate optical signal without the use of external light source. It has demonstrated enhanced optical signal intensity, high SNR, deep penetration depth, and high sensitivity using the internal dual excitation of nanoparticles by both gamma rays and Cerenkov photons.[32,33] To compare with the existing optical image guided surgery, the REF image guided surgery strategy was firstly compared with FMI using a targeted fluorescent probe. Considering indocyanine green (ICG) is the FDA-approved fluorescent probe and has been widely used in clinic in FMI guided surgery, therefore REF image guided surgery was conducted and compared with ICG image guided surgery. Our current study systematically evaluates the performance of REFI for surgical navigation using subcutaneous breast cancer 4 T1 tumor models, orthotopic hepatocellular carcinoma (HCC) tumor-bearing mice, and orthotopic-ectopic HCC tumor-bearing mice, and its performance has been compared to that of FMI.

Methods

Preparation of radiopharmaceuticals and EO nanoparticles

All the radiopharmaceuticals available in clinic including ^{18}F–FDG and ^{11}C–Choline (^{11}C–CHO) were obtained from the Department of Nuclear Medicine, Chinese PLA General Hospital (Beijing, China). EO nanoparticle (Eu_2O_3, 99.9% metal basis, molecular weight = 351.91) was purchased from Aladdin (Shanghai, China) and used as previously described.[32]

Cell culture

Luciferase labeled human well-differentiated HCC cells HepG2-Red-FLuc, luciferase labeled mouse mammary gland adenocarcinoma cells 4 T1-Red-FLuc, and human breast cancer Bcap-37 cells were used for the following experiments. Detailed information can be found in supplemental information.

In vitro imaging

All optical images were acquired with IVIS Kinetic imaging system (PerkinElmer, Waltham, MA) with a 4 × 4 binning, aperture f_{num} of 1. Regions of interest (ROIs) of the corresponding areas were drawn over the optical images, and the average radiances were calculated by the Living Image 3.2 software (PerkinElmer, Waltham, MA, USA), which provides the quantification information, such as the intensities of the optical signals.

Fluorescence of EO nanoparticles (0.107 g) was acquired with 1 s exposure time (w/o excitation: 430 nm, emission: 620 nm). The excitation and emission spectrum of EO nanoparticles were measured using a fluorescence spectrophotometer (Hitachi, Tokyo, Japan). Cerenkov luminescence (CL) of ^{18}F–FDG (277 μCi, 0.1 mL) was acquired with 5 minutes exposure time. Microcentrifuge tubes containing previous two samples were placed abreast (approximately 10 mm apart) and REF image was acquired with 5 minutes exposure time. Emission spectrum of EO nanoparticles was measured by IVIS system using filters from 500 nm to 800 nm. After that, the two samples of ^{18}F–FDG and EO nanoparticles were mixed together. REF image of the mixture was acquired with 20 s exposure time. The spectrum of the mixture was measured by IVIS system using filters from 500 nm to 800 nm.

Different amounts of EO nanoparticles (10^{-3} g, 10^{-5} g, 10^{-7} g, 10^{-9} g, 10^{-12} g) and ^{18}F–FDG with the activity of 1 μCi or 0.1 μCi were separately added into the wells of a black 96-well plate. ^{18}F–FDG with the activity of 1 μCi or 0.1 μCi was used as control. CL of ^{18}F–FDG and REF of the mixtures were acquired with 5 minutes exposure time.

Apoptosis analysis using flow cytometry

Apoptosis staining was conducted using the Dead Cell Apoptosis Kit with Annexin V Alexa Fluor® 488 & Propidium Iodide (PI) - for flow cytometry (Life Technologies, Carlsbad, *CA*). Detailed information can be found in supplemental information.

Hematoxylin and eosin staining

To evaluate the tissue toxicity of EO nanoparticles, the Bcap-37 xenograft mice (n = 4) were sacrificed immediately after *in vivo* imaging for histological examination. Organs were fixed in 4% formalin, and paraffin-embedded sections (4 mm thickness) were prepared for hematoxylin and eosin (H&E) staining. The slices were examined using an inverted microscope

(Leica, Buffalo Grove, IL). The control group (n = 4) was the mice injected with PBS.

Biodistribution and pharmacokinetic study

All animal studies were conducted in compliance with the Fourth Military Medical University Animal Studies Committee (Protocol 20,090,260). BALB/c nude mice and Wistar rats (Vital River, Beijing, China) were used for biodistribution and pharmacokinetic study, respectively. Detailed information can be found in supplemental information.

Establishment of the tumor mice models

Luciferase labeled human well-differentiated HCC cells HepG2-Red-FLuc (PerkinElmer, Waltham, MA) and luciferase labeled mouse mammary adenocarcinoma cells 4 T1-Red-FLuc (PerkinElmer, Waltham, MA) were used to establish tumor mice models. In order to study the performance of REF image-guided cancer surgery and compare with FM image-guided cancer surgery, subcutaneous breast cancer 4 T1 tumor model, orthotopic HCC-bearing mice, and orthotropic-ectopic HCC-bearing mice were established by injecting 1×10^6 4 T1 cells in the mice right upper flank, 5×10^6 HCC cells in the mice liver lobes, and 5×10^6 HCC cells in the mice liver lobes and into the peritoneum, respectively.

Image-guided cancer surgery protocol

The experimental protocol is shown in Figure S1. FM and REF images were all acquired with an aperture f_{num} of 1 and 8 × 8 binning. Excitation and emission filter for fluorescent probes were 745 nm and 840 nm, respectively. Emission filter for REFI was 620 nm. Exposure time for REFI was 5 minutes. Other details were introduced as follows.

REF and FM image-guided cancer surgery of subcutaneous breast cancer 4 T1 tumor model

Seven days after the construction of the mice bearing subcutaneous 4 T1 tumor, the mice (n = 16) were injected with fluorescent molecular probe MMPSense™ 750 FAST (20 mM, 100 μL, PerkinElmer, Waltham, MA) or IntegriSense™ 750 (20 mM, 100 μL, PerkinElmer, Waltham, MA), respectively. Twenty-four hours later, the mice were injected with ^{18}F–FDG (100 μCi, 0.1 mL) and then EO nanoparticles (1 mg/mL, 0.1 mL) intravenously. To compare the performance of REFI for guiding the tumor resection with FMI, FMI and REFI of the mice were immediately performed after the injection. Based on the FM or REF images, the subcutaneous 4 T1 tumor was resected. After the resection, the FM (1 s exposure time) and REF images of the mice and the resected tumor were acquired. The tumor signal-to-normal tissue ratios of REFI and FMI were calculated by dividing the intensities of ROIs obtained from the Living Image 3.2 software, which drawn ROIs over the corresponding areas. Tumors were frozen in the tissue freezing medium (Leica, Buffalo Grove, IL) at −20 °C and resected for microscopic colocalization of tumor biomarkers and EO nanoparticles.

REF and FM Image-guided cancer surgery of orthotopic HCC-bearing mice

Two weeks after the construction of the orthotopic HCC-bearing mice, the mice (n = 4) were injected with ICG (100 mg/L, 100 μL). Twenty four hours later, the mice were injected with ^{11}C–CHO (147 μCi, 0.1 mL) and then EO nanoparticles (0.1 mL, 1 mg/mL) intravenously. The mice received the laparotomy and the REF images were acquired. Based on the REF images, the tumor was resected. REFI of the mice and the resected tumor were performed again. Before and after the resection of the tumor, FMI were acquired with 1 s exposure time. After that, all the organs of the mice were dissected and received for REFI and FMI. If any optical signal presented, tissues would be excised based on the optical images. H&E staining was conducted on the cryosection of resected tumor tissues.

REF and FM image-guided cancer surgery of orthotopic and ectopic HCC-bearing mice

Two weeks after the construction of the orthotopic and ectopic HCC-bearing mice, the mice (n = 4) were injected with ICG (100 mg/L, 100 μL) intravenously. Twenty four hours later, the mice were injected with ^{11}C–CHO (100 μCi, 0.1 mL) and then EO nanoparticles (1 mg/mL, 0.1 mL) intravenously. The mice then received the laparotomy and the REF images were acquired. Based on the REF images, the tumors were resected. Before the resection, the FM images of the mice were also acquired with 2.5 s exposure time. After the first surgical operation, FMI and REF images of the mice and the resected tumors were acquired. Based on the results of REFI, whether there was residual tumor or not was evaluated and the results were compared with FMI. The resected tumors were imaged for photograph, REF images and FM images (5 s exposure time). H&E staining was conducted on the paraffin sections of resected tissues. REF (emission: 540 nm, excitation: 500 nm) and FM images (1 s exposure time, emission: 840 nm, excitation: 745 nm) of the sections were acquired.

Microscopic colocalization of tumor biomarkers and EO nanoparticles

Resected tumors were split into two halves with a lancet. Cryosections and paraffin sections were sliced from the cross section for immunofluorescence staining and H&E staining, respectively. Detailed information can be found in supplemental information.

Statistical analysis

Data were expressed as mean ± standard deviation. Statistical significance was determined using the Student *t* test (Prism v6.0, GraphPad, La Jolla, *CA*). Linear regression was determined using Origin Pro v8.0 (OriginLab, Northampton, MA). Differences between groups were considered significantly if $P \leq 0.05$.

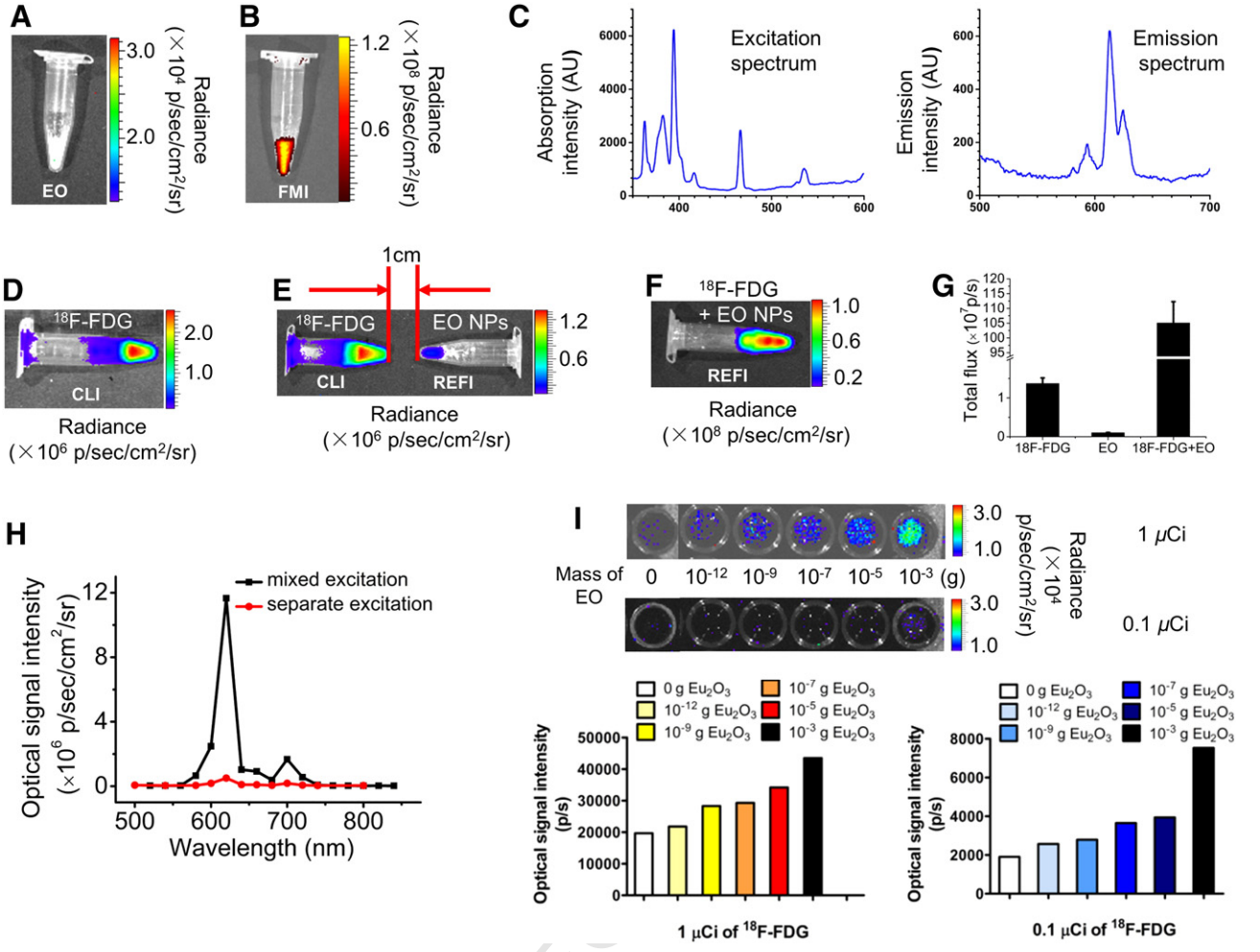

Figure 1. Comparison of CLI and REFI of microcentrifuge tubes and black 96-well plate. **(A)** FMI of the EO nanoparticles (0.107 g) without laser excitation. **(B)** FMI of EO nanoparticles when excited by the laser of 430 nm. The emission filter was 620 nm. **(C)** The excitation and emission spectra of EO nanoparticles. **(D)** CLI of ^{18}F–FDG (277 μCi, 0.1 mL). **(E)** CLI and REFI of the two microcentrifuge tubes contained EO nanoparticles and ^{18}F–FDG approximately 10 mm apart. **(F)** REF image of EO nanoparticles mixed with ^{18}F–FDG. **(G)** Comparison of optical intensity of ^{18}F–FDG, EO and the mixture of ^{18}F–FDG and EO nanoparticles. **(H)** Emission spectra of the mixture of ^{18}F–FDG and EO nanoparticles (mixed excitation) and EO nanoparticles placed close to ^{18}F–FDG (separate excitation). **(I)** REFI of the mixture of EO nanoparticles (10^{-12} g; 10^{-9} g; 10^{-7} g; 10^{-5} g; 10^{-3} g) and ^{18}F–FDG (1 μCi; 0.1 μCi) and CLI of ^{18}F–FDG (1 μCi; 0.1 μCi; no EO nanoparticles) only.

Results

Imaging of microcentrifuge tubes and black 96-well plate

No fluorescent signal was found for the EO nanoparticles without laser excitation (Figure 1, *A*), whereas fluorescent signal emitted when the sample was excited by the laser of 430 nm (Figure 1, *B*). Figure 1, *C* shows the excitation and emission spectra of EO nanoparticles. Multiple characteristic absorption peaks were found at 363, 382, 394, 466 and 535 nm. The maximum emission peak of EO nanoparticles was at 613 nm. ^{18}F–FDG (277 μCi, 0.1 mL) was placed into a microcentrifuge tube and emitted Cerenkov luminescence (Figure 1, *D*). When the microcentrifuge tube contained EO nanoparticles was placed close to ^{18}F–FDG with a distance of approximate 1 cm, intense optical signal of the EO nanoparticles was detected (Figure 1, *E*). The total flux of ^{18}F–FDG and EO nanoparticles were found to be 1.433×10^7 p/s and 1.053×10^6 p/s, respectively. Interestingly, when EO nanoparticles and ^{18}F–FDG were mixed together (Figure 1, *F*), the total flux was measured to be 1.091×10^9 p/s, that was almost 70 times higher than the sum of the optical signals of EO nanoparticles and ^{18}F–FDG. Quantification analysis and comparison of optical signal intensity of ^{18}F–FDG, EO, and the mixture of ^{18}F–FDG and EO are shown in Figure 1, *G*, which clearly demonstrated signal of much higher intensity generated by the mixture of ^{18}F–FDG and EO nanoparticles than their alone.

Emission spectra (Figure 1, *H*) of the mixture of ^{18}F–FDG and EO (mixed excitation, as in Figure 1, *F*) and EO placed close by ^{18}F–FDG (separate excitation, as in Figure 1, *E*) showed that the maximum emission peak of the spectrum was 620 nm for both. CLI of ^{18}F–FDG (1 μCi; 0.1 μCi) and REFI of the mixture of ^{18}F–FDG (1 μCi; 0.1 μCi) and different amount of EO nanoparticles (10^{-12} g; 10^{-9} g; 10^{-7} g; 10^{-5} g; 10^{-3} g) are shown in Figure 1, *I*. It was found that CL signal of ^{18}F–FDG

was very weak at the activity of 1 μCi and almost undetectable at 0.1 μCi (the leftmost images in Figure 1, *I*, mass of EO at 0). Impressively, REF signal was obviously enhanced even when EO added at very low dose (10^{-12} g), and the REF intensities continued to increase along with the increased amount of EO nanoparticles (Figure 1, *I*, quantification analysis panel).

In vitro cell toxicity of EO nanoparticles

Apoptosis assay by flow cytometry was used to evaluate the biocompatibility of EO nanoparticles. Interestingly, only a minority of Bcap-37 cells showed apoptosis and necrosis with the increasing of concentration of EO nanoparticles. At the highest concentration of 400 μg/mL, 1.98% and 6.46% of cells showed apoptosis and necrosis, respectively (Figure S2, *A*, right). While in the control group (0 μg/mL), 0.79% and 2.09% of cells showed apoptosis and necrosis, respectively, which may attribute to the damage of cell membranes caused by trypsin during the harvest of attached cells. The results indicated limited cytotoxicity of EO nanoparticles on Bcap-37 cells.

In vivo toxicity of EO nanoparticles

H&E staining results showed no obvious morphological change in kidneys, lungs, liver, and spleen of the experiment group (Figure S2, *B*) with EO injection compared with the control group.

In vivo blood clearance and biodistribution

In vivo behavior of EO nanoparticles was investigated using the standard ICP-MS analysis. The uptake of EO nanoparticles at 24 h post-injection was obviously higher than that at 0.5 h and 48 h in tumor (Figure S3, *A-C*). Interestingly, EO nanoparticles showed both liver and kidney uptakes, indicating they can be clearly through both hepatobiliary and kidney-urinary systems. As shown in Figure S3, *D*, EO nanoparticles also displayed a blood circulation half-time of 8.93 h. The high uptake of EO nanoparticles by tumor can be attributed to the EPR effect and the long circulation time. Thus REFI can be used for further guiding the surgery of tumors.

REF image-guided cancer surgery of subcutaneous breast cancer 4 T1 tumor model achieved consistent imaging results with FM image-guided cancer surgery

Representative fluorescent image of the mice bearing subcutaneous breast cancer 4 T1 tumor injected with fluorescent molecular probe MMPSense™ 750 FAST is shown in Figure 2, *A* (left). The white arrow indicated the position of the subcutaneous 4 T1 tumor. Based on the fluorescent image, the subcutaneous tumor was resected (Figure 2, *A*; right). The REF images obtained using ^{18}F–FDG and EO nanoparticles of the 4 T1 tumor mice model before and after the tumor resection are shown in Figure 2, *B* (before: left; after: right). It showed that REFI clearly detected the subcutaneous tumor and was able to guide the tumor resection. There was significant difference between the SNR of REFI and FMI (Figure 2, *C*; $P < 0.05$). Results of FM and REF image-guided tumor-removal surgery of 4 T1 tumor mice injected with fluorescent molecular probe IntegriSense™ 750, and comparison of SNR of REFI and FMI are shown in Figure 2, *D-F*, respectively.

Comparison of SNR of REFI and FMI is shown in Figure 2, *G*. SNR of REFI was higher than those of the FMI using two fluorescent probes, especially significantly higher than that of the IntegriSense™ 750. Figure 2, *H* and *J* is the immunofluorescence image of the tumor tissues of the mice injected with MMPSense™ 750 FAST and IntegriSense™ 750, respectively. Immunofluorescence signals indicated that tumor biomarkers (MMP-2 and α_v) were moderately expressed in the tumor tissue, which were in accordance with the results of FMI. Fluorescence of EO nanoparticles showed the intercellular retention of EO nanoparticles in the tumor tissue, which was consistent with the results of REFI. Figure 2, *I* and *K* are the H&E staining results of the resected tumor tissues, respectively.

REF image-guided cancer surgery detected the residual cancer tissue

REF image-guided cancer surgery also detected the orthotopic HCC using ^{11}C–CHO and EO nanoparticles (Figure 3, *A*; left). One HCC tumor was clearly identified. Based on the REF image, the orthotopic tumor was resected. The mouse and the resected tumors were then imaged for REFI again (Figure 3, *A*; right). To compare with FMI, FM images of the mouse before and after the tumor resection were acquired using ICG injected 24 hours ago (Figure 3, *B*). REFI showed much higher SNR than that of FMI (44.05 ± 8.378 *vs.* 2.173 ± 0.1092) (Figure 3, *C*). REFI and FMI of all the mouse organs and the orthotopic HCC are shown in Figure 3, *D* and *E*, respectively. The REF image of the mouse liver is shown in Figure 3, *F*. It was found that there were REF signals in the liver lobe besides the mouse gall bladder. Figure 3, *G* is the FM image of the same mouse liver. Interestingly there was no signal in the liver tissues. SNR of REFI was much higher than that of FMI (Figure 3, *H*, $p<0.05$). Based on the REF image of the mouse liver, the residual cancer tissue was resected. After the resection, the photograph and the REF image of the mouse liver is shown in Figure 3, *I*, respectively. H&E of the orthotopic HCC and surgical margin verified the first and the second resected tissues were HCC (Figure 3, *J* and *K*).

REF image-guided cancer surgery detected invisible ultra-small size tumor

REF image-guided cancer surgery was further conducted on the orthotopic and ectopic HCC-bearing mice (n = 4). After the laparotomy, FMI of the mice was performed using ICG at 24 h post-injection. FM image showed that there were much fluorescence in the whole mice body (Figure 4, *A*), which did not detect any tumors. However, REF image clearly detected three tumors using ^{11}C–CHO and EO nanoparticles (Figure 4, *B*). The yellow arrows showed the positions of the three tumors. The SNR of REFI was much higher than that of FMI (83.98 ± 25.35 *vs.* 1.183 ± 0.03637; Figure 4, *C*, $p<0.05$). Based on the REF image, three tumors were resected and acquired for REF image (Figure 4, *D*). After tumor resection, the mice were immediately imaged for FMI (Figure 4, *E*) and for REFI (Figure 4, *F*). There was high fluorescent signal in the whole mice body (Figure 4, *E*). Interestingly, an invisible ultra-small size tumor (0.99

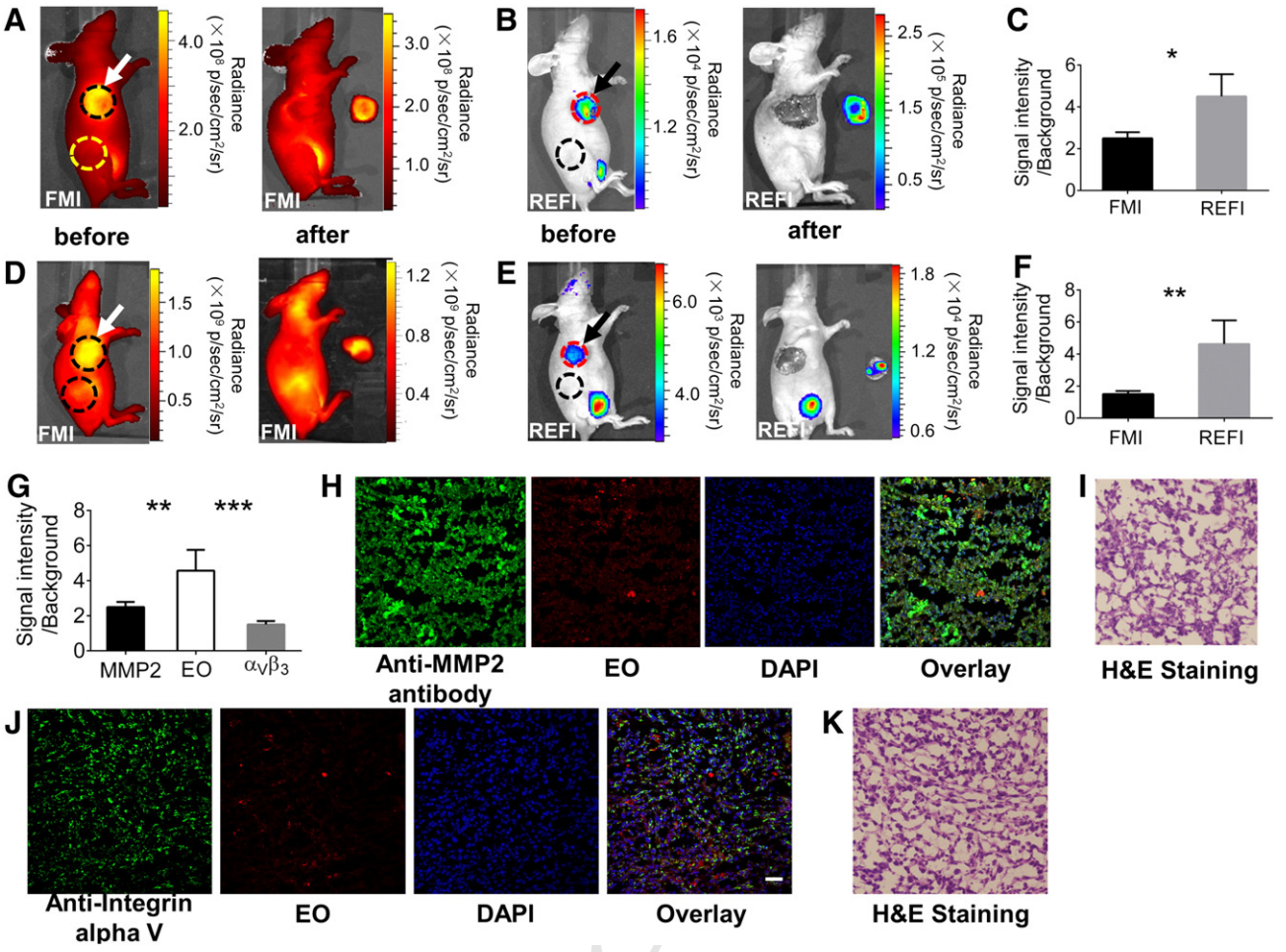

Figure 2. Comparison of FM image-guided cancer surgery and REF image-guided cancer surgery of subcutaneous breast cancer 4 T1 tumor model (n = 4 per group). **(A)** Representative FMI of the tumor mouse model (left) injected with MMPSense™ 750 FAST. The white arrow indicated the position of the tumor. Based on the fluorescent image, the subcutaneous tumor was resected (right). **(B)** Representative REF images of the mouse injected with ^{18}F–FDG and EO nanoparticles before and after the tumor resection. **(C)** Comparison of SNR of FMI using MMPSense™ 750 FAST and REFI using ^{18}F–FDG and EO nanoparticles. **(D)** FMI of the mouse injected with IntegriSense™ 750 before and after the tumor resection (before: left; after: right). The white arrow indicated the position of the subcutaneous 4 T1 tumor. **(E)** The representative REF images of the mouse injected with ^{18}F–FDG and EO nanoparticles before and after the tumor resection (before: left; after: right). **(F)** Comparison of SNR of FMI using IntegriSense™ 750 and REFI using ^{18}F–FDG and EO nanoparticles. **(G)** Comparison of SNR of REFI using ^{18}F–FDG and EO nanoparticles and FMI using two different kinds of fluorescent probes. Both **(H)** and **(J)** contain immunofluorescence results of the tumor biomarkers (MMP-2 and α_v), fluorescence of EO nanoparticles, DAPI stained nuclei and the overlays of the resected tumor tissues dissected from the mouse which was injected with MMPSense™ 750 FAST or IntegriSense™ 750. **(I)** and **(K)** are the H&E results of the resected tumor tissues respectively.

mm × 0.61 mm) was detected by REFI. SNR of the REFI was significantly higher than that of FMI (Figure 4, *G*). Based on the REF image, the micro-lesion was resected. After the resection, the mice were imaged for REFI again and no signals were detected (Figure 4, *H*). Photograph of the representative mouse is shown in Figure 4, *I*. Photograph, REFI, and FMI of the four resected tumors are displayed in Figure 4, *J-L*, respectively. H&E, REFI, FMI of the sectioned slices of the micro-lesion tissue is depicted in Figure 4, *M-O*, respectively.

Retaining of EO nanoparticles in the tumor vessels

H&E results showed there were many nanoparticles retaining in the tumor vessels of the mice bearing Bcap37 tumors (Figure S4). The black dots were the EO nanoparticles. There were also some nanoparticles retaining in the tumor tissues, though much less than in the blood vessels.

Discussion

Whether the tumor can be surgically accurately removed is directly related to tumor recurrence and metastasis. Precise tumor resection is closely related to the prognosis and survival of cancer patients.[34] Current clinical surgical navigation research primarily focuses on FMI. The main problem is the high background signal, low SNR caused by the autofluorescence produced by the external laser excitation. Our goal is to develop a novel imaging technique to improve the SNR of the tumor

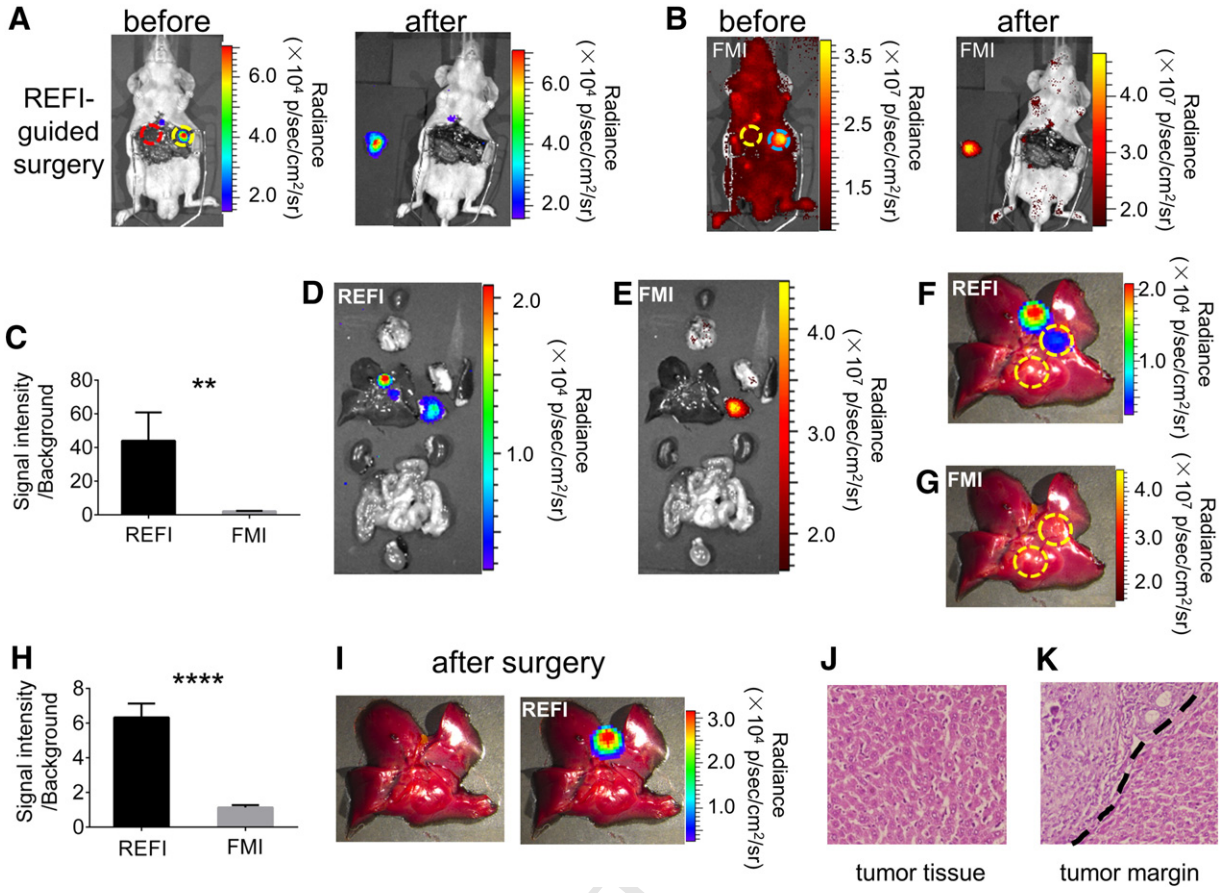

Figure 3. REF image-guided cancer surgery of the orthotopic HCC tumor-bearing mice (n = 4 per group). **(A)** Representative REFI of the mouse after the laparotomy (left). After the REF image-guided cancer surgery, the mouse and the resected tumor were also imaged for REFI (right). **(B)** Representative fluorescent images of the mouse before and after the tumor resection. **(C)** Comparison of SNR of REFI and FMI. **(D)-(E)** REFI and FMI of all the organs and the orthotopic HCC. **(F)-(G)** Representative REF and FM image of the mouse liver, respectively. **(H)** Comparison of quantification of SNR of REFI and FMI of the mouse liver. **(I)** Photograph and REF image of the mouse liver after the tumor second resection, respectively. **(J)-(K)** H&E of the orthotopic HCC and surgical margin, respectively.

imaging and detect the tumors as much as possible to realize the precise resection.

This work presents a novel radiopharmaceutical-excited fluorescence (REF) image-guided cancer surgery. The REFI strategy employs dual excitation of EO nanoparticles by both gamma rays and Cerenkov luminescence (CL) emitted from radiopharmaceuticals to generate strong near-infrared fluorescence for image-guided cancer surgery. Importantly, REFI combines the active and specific targeting of radiopharmaceuticals (such as ^{18}F–FDG, ^{11}C–CHO) and passive targeting of EO nanoparticles *via* EPR effect, and therefore it leads to high imaging sensitivity and specificity.[32] In this work, experimental results further demonstrate that REF image-guided cancer surgery can detect the residual cancer tissues as well as invisible micro-lesions (Figures 3 and 4).

Firstly, through *in vitro* cell experiments, the toxicity of EO nanoparticles in cells was tested. The results show that EO nanoparticles have no significant impact to the cell to induce cell apoptosis (Figure S2, *A*).

Then *in vitro* experiment was designed to demonstrate that the EO nanoparticles illuminated when excited by radiopharmaceuticals, suggesting its possible usage for *in vivo* imaging of tumor mice models. As expected, EO nanoparticles alone do not produce any light without laser excitation (Figure 1, *A*). Under laser illumination, EO nanoparticles generate intense fluorescence (Figure 1, *B*). More interestingly, under the irradiation of radiopharmaceuticals, near-infrared fluorescence was produced with maximum emission peak at 620 nm (red; Figure 1, *H*). By mixing the ^{18}F–FDG and EO nanoparticles, strong near-infrared fluorescent light emits (Figure 1, *F*) and its peak is 620 nm (black; Figure 1, *H*). The total flux is almost 70 times higher than the sum of the optical signals of EO nanoparticles and ^{18}F–FDG alone. Further study also indicated that EO of very low dose can be excited by radiopharmaceuticals of very low dose to produce optical signal (Figure 1, *I*).

Experiment results of the mice bearing subcutaneous 4 T1 breast cancer shows that REF-image guided surgery can achieve similar results as FM-image guided surgery, and subcutaneous tumors can be successfully identified and removed using both approaches. H&E staining results demonstrate the resected tissue is tumor tissues. The feasibility of REFI surgical navigation has been validated. Interestingly, the results show that SNR of REFI

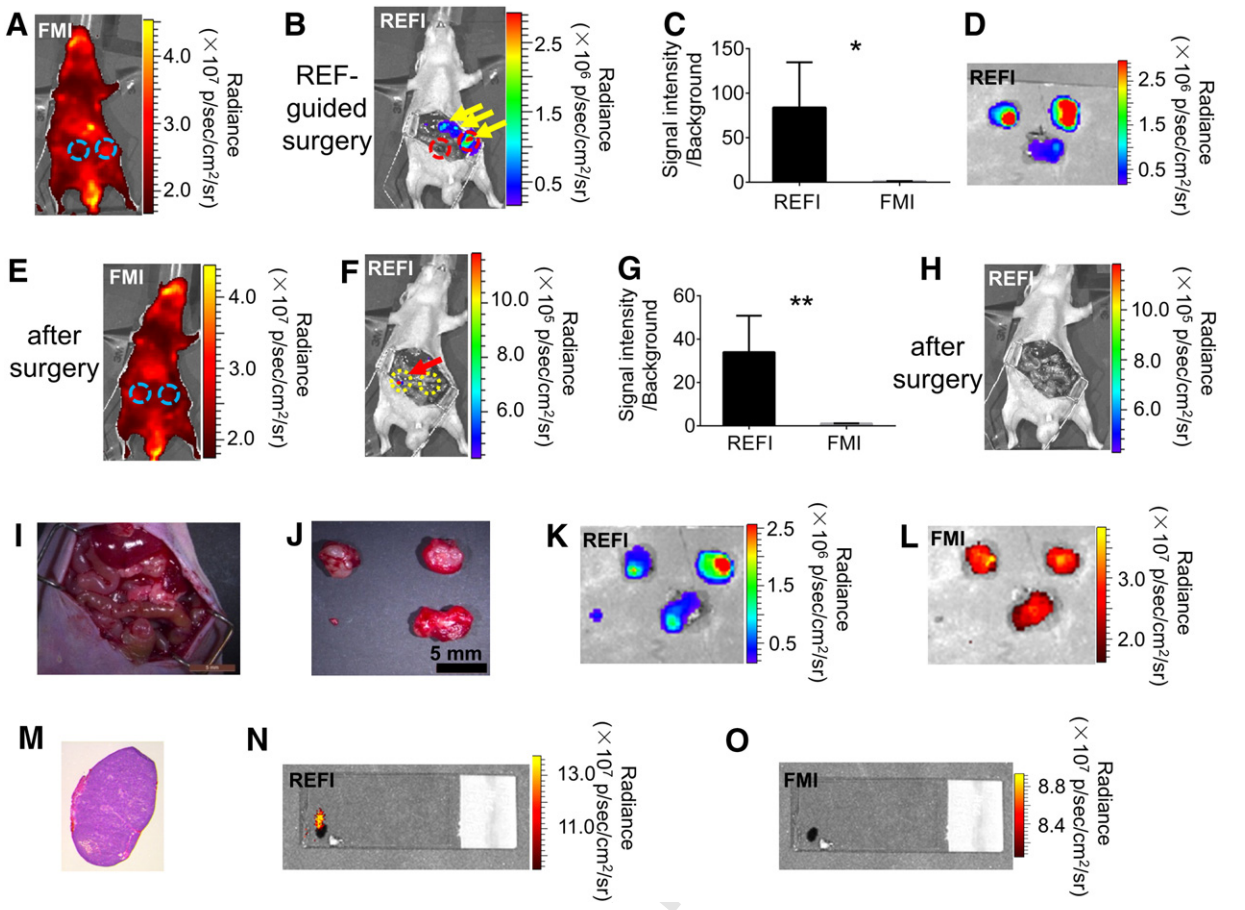

Figure 4. REF image-guided cancer surgery of the orthotopic and ectopic HCC tumor-bearing mice (n = 4 per group). **(A)** FMI of the mouse after the laparotomy. **(B)** REF image of the mouse after the laparotomy. The yellow arrows showed the position of the three tumors. **(C)** The comparison of quantification of SNR of REFI and FMI. **(D)** REF image of the three resected tumors. **(E)** The fluorescent image of the mouse after three tumor resection. **(F)** REFI of the mouse after three tumor resection. The red arrow showed the position of the invisible ultra-small size tumor. **(G)** Comparison of SNR of the micro-lesion of REFI and FMI. **(H)-(I)** REF image and photograph of the mouse after the micro-lesion was resected, respectively. **(J)-(L)** Photograph, REFI, and FMI of the four resected tumors, respectively. **(M)-(O)** H&E, REFI, FMI of the sectioned slices of the tumor tissue of the micro-lesion.

is higher than that obtained through FMI, demonstrating the advantages of REFI over FMI. It should be pointed out that REFI surgical navigation can likely be carried out for a variety of tumor imaging, not limited to tumor types reported in this study, because ^{18}F–FDG can target a variety of tumors through specific accumulation and EO nanoparticles can also accumulate in tumor through EPR effects.

The experiment of orthotopic liver tumor mouse model confirmed REFI not only detected the orthotopic liver tumor and successfully guided the tumor resection, but also detected the residual tumor tissue. In comparison, FMI only detected orthotopic liver tumor (Figure 3). The experimental results demonstrated the superiority of REFI in the detection of residual tumor tissues over FMI.

For the experiment of the orthotopic and ectopic HCC tumor-bearing mice, ICG was chosen as the fluorescent probe for FM image-guided cancer surgery because ICG is widely used in clinical liver cancer imaging. It was found that, after laparotomy, REFI detected three tumors in the abdominal cavity, and thus all of these three tumors were dissected. After the tumor removal, the mice received FMI and REFI again. Interestingly, FMI did not find any signal, while REFI identified an invisible tiny tumor (less than 1 mm) in the abdominal cavity, as shown in Figure 4, *F*. The reason why REFI can find the invisible tiny tumor which FMI cannot detect was correlated with the high SNR of REFI. The size of the tumor detected by REFI is 0.99 mm × 0.61 mm, smaller than that described in the literature.[32]

In this study, ^{18}F–FDG and ^{11}C–CHO were used in the experiment. In the future work, other radionuclides, such as the therapeutic alpha and beta emitters, will be considered to be employed for the REFI experiment. Furthermore, active targeting with the EO nanoparticles labeled by the specific biomarkers will be constructed.

In short, this study presents a novel optical image-guided cancer surgery strategy using nanoparticle-mediated radiopharmaceutical-excited fluorescence molecular imaging, which employs the internal dual excitation of EO nanoparticles by both gamma rays and Cerenkov luminescence of radiopharmaceuticals. REF image-guided cancer surgery technique exhibits the excellent performance of detecting invisible

ultra-small size tumor (less than 1 mm) and residual cancer tissue. Our study demonstrates the high potential of the novel REF image-guided cancer surgery technique for precise tumor resection.

Appendix A. Supplementary data

Supplementary data to this article can be found online at http://dx.doi.org/10.1016/j.nano.2017.01.005.

References

1. van der Vorst JR, Schaafsma BE, Hutteman M, Verbeek FPR, Liefers GJ, Hartgrink HH, et al. Near-infrared fluorescence-guided resection of colorectal liver metastases. *Cancer* 2013;**119**:3411-3418.
2. Tsujimoto H, Yaguchi Y, Kumano I, Takahata R, Ono S, Hase K. Successful gastric submucosal tumor resection using laparoscopic and endoscopic cooperative surgery. *Surg* 2012;**36**:327-330.
3. Antaris AL, Chen H, Cheng K, Sun Y, Hong G, Qu C, et al. A small-molecule dye for NIR-II imaging. *Nat Mater* 2016;**15**:135-142.
4. Nguyen QT, Olson ES, Aguilera TA, Jiang T, Scadeng M, Ellies LG, et al. Surgery with molecular fluorescence imaging using activatable cell-penetrating peptides decreases residual cancer and improves survival. *S A* 2010;**107**:4317-4322.
5. Sampath L, Kwon S, Hall MA, Price RE, Sevick-Muraca EM. Detection of cancer metastases with a dual-labeled near-infrared/positron emission tomography imaging agent. *Transl Oncol* 2010;**3**:307-317.
6. Liberale G, Vankerckhove S, Caldon MG, Ahmed B, Moreau M, Nakadi I, et al. Fluorescence imaging after indocyanine green injection for detection of peritoneal metastases in patients undergoing cytoreductive surgery for peritoneal carcinomatosis from colorectal cancer: a pilot study. *Ann Surg* 2016;**264**:1110-1115.
7. van Dam GM, Themelis G, Crane LM, Harlaar NJ, Pleijhuis RG, Kelder W, et al. Intraoperative tumor-specific fluorescence imaging in ovarian cancer by folate receptor-alpha targeting: first in-human results. *Nat Med* 2011;**17**:1315-1319.
8. Marbacher S, Klinger E, Schwyzer L, Marbacher S, Klinger E, Schwyzer L, et al. Use of fluorescence to guide resection or biopsy of primary brain tumors and brain metastases. *Neurosurg Focus* 2014;**36**e10.
9. Stoffels I, Dissemond J, Pöppel T, Schadendorf D, Klode J. Intraoperative fluorescence imaging for sentinel lymph node detection. *JAMA Surg* 2015;**150**e617.
10. Brouwer OR, van den Berg NS, Matheron HM, van der Poel HG, van Rhijn BW, Bex A, et al. A hybrid radioactive and fluorescent tracer for sentinel node biopsy in penile carcinoma as a potential replacement for blue dye. *Eur Urol* 2014;**65**:600-609.
11. Bu L, Shen B, Cheng Z. Fluorescent imaging of cancerous tissues for targeted surgery. *Adv Drug Deliv Rev* 2014;**76**:21-38.
12. Thorek DLJ, Robertson R, Bacchus WA, Hahn J, Robertson R, Bacchus WA, et al. Cerenkov imaging-a new modality for molecular imaging. *Nucl Med Mol Imaging* 2012;**2**e163.
13. Keereweer S, Van Driel PBAA, Snoeks TJA, Kerrebijn JDF, Baatenbg de jong RJ, Vahrmeijer AL, et al. Optical image-guided cancer surgery: challenges and limitations. *Clin Cancer Res* 2013;**19**:3745-3754.
14. Nguyen QT, Tsien RY. Fluorescence-guided surgery with live molecular navigation a new cutting edge. *Nat Rev Cancer* 2013;**13**:653-662.
15. Liu HG, Ren G, Miao Z, Zhang XF, Tang X, Han PZ, et al. Molecular optical imaging with radioactive probes. *PLoS One* 2010;**5**e9470.
16. Ruggiero A, Holland JP, Lewis JS, Grimm J. Cerenkov luminescence imaging of medical isotopes. *J Nucl Med* 2010;**51**:1123-1130.
17. Robertson R, Germanos MS, Li C, Mitchell GS, Cherry SR, Silva MD. Optical imaging of Cerenkov light generation from positron-emitting radiotracers. *Phys Med Biol* 2009;**54**:355-365.
18. Spinelli AE, Boschi F. Novel biomedical applications of Cerenkov radiation and radioluminescence imaging. *Phys Med* 2015;**31**:120-129.
19. Hu Z, Liang J, Yang W, Fan W, Li C, Ma X, et al. Experimental Cerenkov luminescence tomography of the mouse model with SPECT imaging validation. *Opt Express* 2010;**18**:24441-24450.
20. Hu Z, Ma X, Qu X, Yang W, Liang J, Wang J, et al. Three-dimensional noninvasive monitoring iodine-131 uptake in the thyroid using a modified Cerenkov luminescence tomography approach. *PLoS One* 2012;**7**e37623.
21. Xu Y, Chang E, Liu H, Jiang H, Gambhir SS, Cheng Z. Proof-of-concept study of monitoring cancer drug therapy with cerenkov luminescence imaging. *J Nucl Med* 2012;**53**:312-317.
22. Robertson R, Germanos MS, Manfredi MG, Smith PG, Silva MD. Multimodal imaging with (18)F-FDG PET and Cerenkov luminescence imaging after MLN4924 treatment in a human lymphoma xenograft model. *J Nucl Med* 2011;**52**:1764-1769.
23. Thorek DL, Ogirala A, Beattie BJ, Grimm J. Quantitative imaging of disease signatures through radioactive decay signal conversion. *Nat Med* 2013;**19**:1345-1350.
24. Hu Z, Yang W, Ma X, Ma W, Qu X, Liang J, et al. Cerenkov luminescence tomography of aminopeptidase N (APN/CD13) expression in mice bearing HT1080 tumors. *Mol Imaging* 2013;**12**:173-181.
25. Thorek DL, Das S, Grimm J. Molecular imaging using nanoparticle quenchers of Cerenkov luminescence. *Small* 2014;**10**:3729-3734.
26. Spinelli AE, Lo MS, Calandrino R, Sbarbati A, Boschi F. Optical imaging of Tc-99 m-based tracers: in vitro and in vivo results. *J Biomed Opt* 2011;**16**:275-277.
27. Thorek DL, Riedl CC, Grimm J. Clinical Cerenkov luminescence imaging of 18F-FDG. *J Nucl Med* 2014;**55**:95-98.
28. Liu H, Carpenter CM, Jiang H, Pratx G, Sun C, Buchin MP, et al. Intraoperative imaging of tumors using Cerenkov luminescence endoscopy: a feasibility experimental study. *J Nucl Med* 2012;**53**:1579-1584.
29. Carpenter CM, Ma X, Liu H, Sun C, Pratx G, Wang J, et al. Cerenkov luminescence endoscopy: improved molecular sensitivity with β− emitting radiotracers. *J Nucl Med* 2014;**55**:1905-1909.
30. Kothapalli SR, Liu H, Liao JC, Cheng Z, Gambhir SS. Endoscopic imaging of Cerenkov luminescence. *Biomed Opt Express* 2012;**3**:1215-1225.
31. Song T, Liu X, Qu Y, Liu H, Bao C, Leng C, et al. A novel endoscopic Cerenkov luminescence imaging system for intraoperative surgical navigation. *Mol Imaging* 2015;**14**:443-449.
32. Hu Z, Qu Y, Wang K, Zhang X, Zha J, Song T, et al. In vivo nanoparticle-mediated radiopharmaceutical-excited fluorescence molecular imaging. *Nat Commun* 2015;**6**:7560.
33. Hu Z, Zhao M, Qu Y, Zhang X, Zhang M, Liu M, et al. In vivo three-dimensional radiopharmaceutical excited fluorescence tomography. *J Nucl Med* 2016, http://dx.doi.org/10.2967/jnumed.116.180596.
34. Harmsen S, Huang R, Wall MA, Karabeber H, Samii JM, Spaliviero M, et al. Surface-enhanced resonance Raman scattering nanostars for high-precision cancer imaging. *Sci Transl Med* 2015;**7**:271ra7.